Corrosion Science 205 (2022) 110463

Contents lists available at ScienceDirect

Corrosion Science

journal homepage: www.elsevier.com/locate/corsci

A new look on the corrosion mechanism of magnesium: An EIS investigation at different pH

Abdelmoheiman Zakaria Benbouzid [a,b,*], Maurilio Pereira Gomes [a,c], Isolda Costa [c], Oumaïma Gharbi [a,b,*], Nadine Pébère [d], Jesualdo Luiz Rossi [c], Mai T.T. Tran [b], Bernard Tribollet [b], Mireille Turmine [a,b], Vincent Vivier [a,b,*]

[a] Sorbonne Université, CNRS, Laboratoire de Réactivité de Surface, Paris, France
[b] Sorbonne Université, CNRS, Laboratoire Interfaces et Systèmes Electrochimiques, Paris, France
[c] Instituto de Pesquisas Energéticas e Nucleares, Centro de Ciência e Tecnologia de Materiais, Av. Prof. Lineu Prestes, 2242, Cidade Universitária, CEP 0508-000, São Paulo, SP, Brazil
[d] CIRIMAT, Université de Toulouse, CNRS, INPT, UPS, ENSIACET, 4, allée Emile Monso, BP 44362, 31030 Toulouse Cedex 4, France

ARTICLE INFO

Keywords:
Magnesium
Corrosion mechanism
Negative difference effect (NDE)
Adsorbed intermediates
Electrochemical Impedance Spectroscopy
Impedance modelling

ABSTRACT

This study investigates the electrochemical impedance diagrams obtained for a Mg electrode in a sodium sulphate solution at different pHs. A comprehensive model, independent of the pH range, with the presence of two adsorbed intermediates accounting for the anodic dissolution and the cathodic reaction was proposed to explain the singular behaviour of Mg at low pH values. It was also shown that, in acidic media, the contribution of the double layer as well as the cathodic partial reaction must be considered, whereas at higher pH values the oxide/hydroxide layer plays a significant role and slows down the magnesium corrosion rate.

1. Introduction

The corrosion mechanisms of magnesium and its alloys have been widely investigated and discussed in the literature, under different conditions using a large variety of electrochemical and surface analysis techniques [1–18]. Many articles, including reviews, have been published aiming at clarifying the proposed corrosion mechanisms and to give new insights for the development of the corrosion protection of these materials [19–30]. Despite of all the knowledge gathered about Mg corrosion, its corrosion mechanism, and in particular the anomalous anodic hydrogen evolution (known as negative different effect – NDE), are considered as enigmatic and are still not clearly understood [18,30,31]. This is because of the complexity of the chemistry and electrochemistry of magnesium in aqueous solutions [32], which may involve, depending on the authors [30], an oxide film on the surface of Mg [33–35], water dissociation [32,36–42], the NDE [16–18,43–47], adsorption of species, monovalent magnesium ion (Mg^{+}) formation [9–15,48], interfacial pH variation [17,49–52], and precipitation of corrosion products [9–15, 52].

Many attempts have been made to understand and identify the various phenomena occurring at the Mg/electrolyte interface with a particular emphasis on the NDE analysis [30]. These works have led to the suggestion of several mechanisms, based on the formation of intermediate species, such as the univalent Mg^{+} ion model [19–27,53–55], the partially protective surface film model [3,56,57] or the incomplete film univalent Mg^{+} ion model [19,30] corresponding to the combination of these two mechanisms [30]. For the latter, Mg surface is partially protected by a thin oxide film and film-free area increases with increasing the anodic potential or current [30]. On the bare surface, Mg is first electro-oxidized to form a Mg^{+} species which, in turn, is either electro-oxidized to form Mg^{2+} or chemically reacts with water or hydronium cations leading to hydrogen evolution [30]. This chemical reaction could be the reason for the anodic hydrogen evolution but is based on the presence of the monovalent Mg^{+} which, to the best of our knowledge, has not been detected when investigating the corrosion of Mg in aqueous solutions [30,54,58]. However, Al Bacha et al., provided for the first time, evidence of the formation of an univalent intermediate on the metal surface, MgOH and/or MgH_{ads}^{+} using in situ Raman spectroscopy [59], whereas Samaniego et al. disproved the existence of Mg^{+} as stable species in the aqueous solution [58] when revisiting the Petty

* Corresponding authors at: Sorbonne Université, CNRS, Laboratoire de Réactivité de Surface, Paris, France
E-mail addresses: benbouzid.abdelmoheiman.zakaria@gmail.com (A.Z. Benbouzid), oumaima.gharbi@sorbonne-universite.fr (O. Gharbi), vincent.vivier@sorbonne-universite.fr (V. Vivier).

https://doi.org/10.1016/j.corsci.2022.110463
Received 2 May 2022; Received in revised form 18 June 2022; Accepted 23 June 2022
Available online 29 June 2022

experiment [54] with the help of Raman spectroscopy. Studies based on first-principle modelling are in contradiction with each other regarding the theoretical existence of such an intermediate entity [38,60–63], but disagreements are usually explained by short life of the Mg^+ [30].

Similarly, another model has been proposed based on the adsorption of the intermediate species, Mg^+, on the film-free areas, since this cation is believed to be highly reactive with water and thus could not exist in the solution as a hydrated compound [6,17,45]. Moreover, in this model, the Mg corrosion is controlled mainly by the development of a thin oxide film on the Mg surface [6,17,45]. At this point, it should be mentioned that other mechanisms aiming always to clarify the different experimental observations, have also been proposed such as the magnesium hydride model [30,64–70], the enhanced cathodic catalytic activity [30,71,72], the impurity particle cathode model [16,30,73,74] and, the Mg*H/Mg*OH catalysts model [36,37,39,40], but they partially account for the whole observations reported in the literature [30].

It is well-known that magnesium dissolves to a greater extent under acidic or neutral conditions than in alkaline media [4,46]. In alkaline solutions, the formation of a protective magnesium oxide/hydroxide film prevents its dissolution [4,35,46,52]. Moreover, the pH at the Mg/solution interface tends to increase to a value of about 11, since the cathodic reaction produces hydroxide ions or consumes protons [4,46].

The complex chemistry of the Mg corrosion as function of pH and electrolyte composition can explain why so many types of mechanisms have been proposed [9–14,75–80]. Generally, the following mechanisms are involved in the dissolution of divalent metals, M(II) [81]:

The aquo-ligand mechanism:

$$M \rightarrow M^+_{ads} + e^- \quad (a1)$$

$$M^+_{ads} \rightarrow M^{2+}_{aq} + e^- \quad (a2)$$

The hydroxo-ligand mechanism:

$$M + H_2O \rightarrow MOH_{ads} + H^+ + e^- \quad (b1)$$

$$MOH_{ads} \rightarrow MOH^+_{aq} + e^- \quad (b2)$$

The aniono-ligand mechanism:

$$M + A^- \rightarrow MA_{ads} + e^- \quad (c1)$$

$$MA_{ads} \rightarrow MA^+_{aq} + e^- \quad (c2)$$

In the hydroxo-ligand mechanism, it is common to consider MOH_{ads} as the first intermediate involved in the formation of a passivation layer following the reaction [81]:

$$MOH_{ads} + H_2O \rightarrow M(OH)_2 + H^+ + e^- \quad (b3)$$

Electrochemical impedance spectroscopy (EIS) is a powerful in situ technique to investigate the Mg corrosion mechanism which involves multiple steps with adsorbed intermediate species [1,4,6,13,17,35,81,82]. It provides accurate information about the different processes occurring at the metal/electrolyte interface, and gives access to several parameters of the system. Here, it must be emphasized that *ex situ* surface analysis, even at the nanoscale, such as transmission electron microscopy (TEM) or X-ray photoelectron spectroscopy (XPS) cannot be used to detect the adsorbed intermediate species.

As far as we know, the corrosion of magnesium at the early stages in highly acidic media, has never been investigated by means of EIS [45,46,49–52], and so far, the existence of two inductive loops in the low frequency range, has been reported only for Mg alloys [83–87] and has generally been ascribed to corrosion initiation and adsorption of corrosion products in the pits [83], localized or micro-galvanic corrosion and corrosion associated with porosity [84], hydrogen corrosion process, and initiation of pitting [85], corrosion product desorption and chemical reaction between Mg^+ and H_2O [86], as well as local disruption of passive layer contributing to localized corrosion and adsorption of hydrogen atoms [87]. In all these studies, the inductive behaviour has not been deeply investigated and the description of the corrosion mechanism was only limited to the use of equivalent electrical circuits.

The aim of the present work is to discuss new experimental results on the pH dependence of the Mg corrosion, at the early stages of immersion in sodium sulphate solutions using EIS. From impedance data analysis, a comprehensive model accounting for the adsorption of hydrogen atoms is proposed to complete the existing mechanism [6,17] and thus, to fully describe all the time constants observed experimentally in the whole investigated pH range.

2. Experimental

The experiments were performed in naturally aerated 1 M sodium sulphate (Na_2SO_4) solutions, acidified with diluted H_2SO_4 solution to a pH of 7.7, 2.9 and 1.8 at 25 °C. It can be mentioned that Mg corrosion is relatively insensitive to the oxygen concentration because the reduction of water molecules or protons are the main cathodic reactions involved in the corrosion process.

Electrolytes were prepared using anhydrous sodium sulphate (99%, Acros Organics), sulphuric acid (96% for analysis, Carlo Erba Reagents) and deionized water. A volume of 50 mL of Na_2SO_4 solution was used for the EIS measurements.

The pH of the different solutions and pH monitoring were conducted at 25 °C using a pH meter and a pH electrode from Radiometer analytical.

It is worth mentioning that during the impedance measurement, the pH increases but insignificantly from 1.8 to 1.9 for the first 2 h (corresponding to 30 min holding time at E_{corr} followed by 1.5 h for EIS measurement), then from 1.9 to 2.2 after 3 h (corresponding to 1.5 h holding time at E_{corr} + 1.5 h EIS measurement). This will be further discussed in the following section.

All the experiments were performed using a Gamry Ref 600+ potentiostat, an Mg (99.9%, Goodfellow) rotating disk electrode (5 mm in diameter) at 1000 rotations per minute (rpm), a saturated mercury sulphate reference electrode (MSE - $E = 0.64$ V/SHE at 25 °C) and a large platinum grid as a counter electrode. The temperature of the electrolytic solutions was controlled to 25 ± 0.5 °C by using a water circulating bath. The impurity contents of the Mg, the working electrode preparation as well as the polishing and cleaning of the Mg surface are reported elsewhere [17].

EIS measurements were conducted using a potentiostatic regulation at the corrosion potential (E_{corr}) after a holding time of 30 min. The measurements consisted in applying a 10 mV_{rms} amplitude perturbation in a frequency domain ranging from 100 kHz to few tens mHz with an acquisition of 8 points per frequency decade. The measured impedance data was tested for compliance with the Kramers–Kronig relations [82,88] using the Gamry software. At very high frequencies, the impedance diagrams are influenced by the geometry effect of the rotating disk electrode on the current and potential distributions [82], whereas depending on the pH, data accuracy at very low frequencies may be not sufficient due to the low stationarity of the electrochemical systems and thus in some case these points were disregarded. Reproducibility was checked from several experiments. Despite the high reactivity of the Mg and bubbles formation at the surface of the electrode, partially removed by the electrode rotation, high reproducibility was achieved. The results presented are representative of each experimental condition.

The anodic and cathodic potentiodynamic curves, for the pH = 1.8

solution, were plotted separately after a holding time of 30 min at E_{corr}, from E_{corr} - 10 mV to E_{corr} + 250 mV and from E_{corr} + 10 mV to E_{corr} - 250 mV. A slow sweep rate of 0.1 mV s^{-1} was used to ensure quasi steady-state measurements. The polarization curves were corrected from the ohmic drop using the electrolyte resistance, R_e, graphically determined from the EIS diagrams as the high frequency limit of the real part (R_e was about 2.1–2.2 Ω cm^2 depending on the position of the reference electrode).

3. Results and discussion

3.1. Electrochemical impedance measurements

3.1.1. Impedance diagrams at E_{corr}

Fig. 1 shows the impedance diagrams for the Mg electrode for different initial pH (1.8, 2.9 and 7.7). For a pH of 7.7 (Fig. 1**a**), a classical three-time constants impedance diagram, usually observed for a Mg electrode in neutral or alkaline sodium sulphate solution [1,6,17], was obtained. The first capacitive loop, in the high frequency range, corresponds to the charge transfer resistance in parallel with the interfacial capacitance [1,6,17]. In alkaline media, this interfacial capacitance is mainly dominated by the response of the thin oxide layer and thus, the contribution of the double layer can be neglected [1,6,17,35]. The second time constant, in the medium frequency range, corresponds to the diffusion of Mg^{2+}, or other species, e.g., OH^-, inside the porous $Mg(OH)_2$ corrosion layer formed on top of the oxide layer (MgO) [6,17,45] when the pH is sufficiently high [4,35,46,52]. In the low frequency range, the inductive loop corresponds to the relaxation of adsorbed intermediates [81,82], very likely adsorbed monovalent magnesium cations "Mg^+_{ads}" as previously stated in [6,17,45].

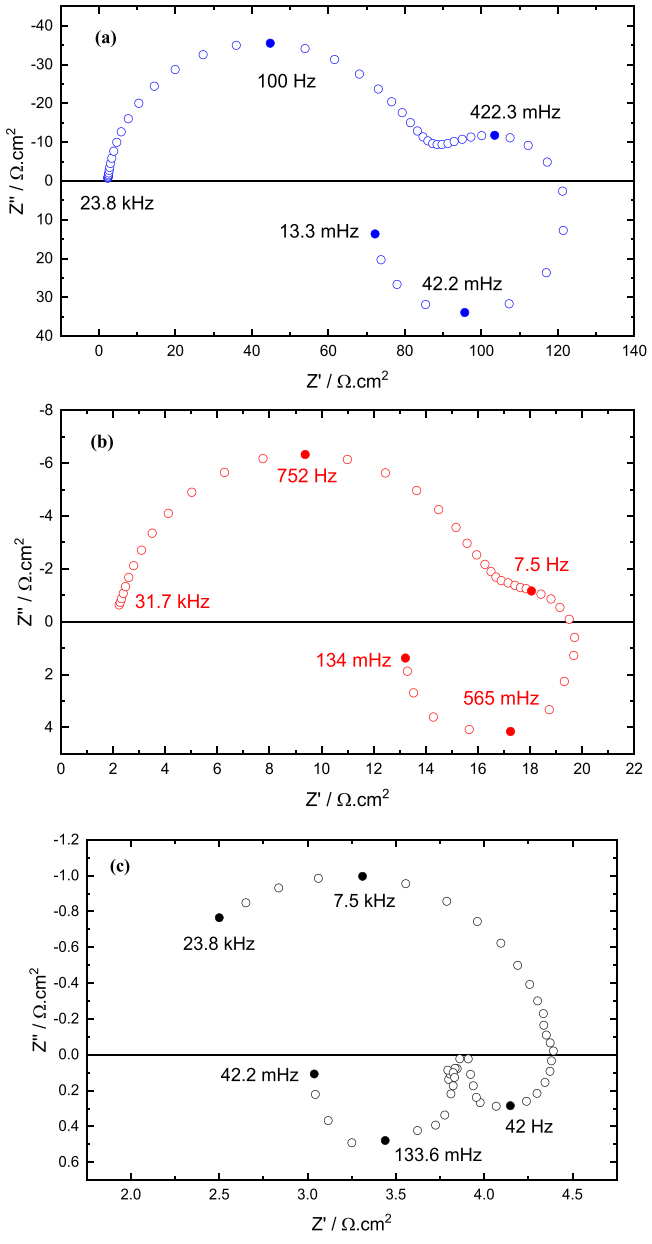

Fig. 1. Electrochemical impedance diagrams (Nyquist representation) of Mg after 30 min immersion at E_{corr} in 1 M Na_2SO_4 solution at different pH values (electrode rotation rate Ω = 1000 rpm): (a) pH = 7.7; (b) pH = 2.9; (c) pH = 1.8.

The use of a monovalent intermediate is in agreement with the Marcus theory as discussed in detail by Koper [89], stating that a monoelectronic transfer is more favoured than a simultaneous transfer of two electrons. Indeed, the latter requires an activation energy which is four times larger than in a monoelectronic transfer confirming that the route with an adsorbed intermediate should be preferred [89]. In addition, according to the quantum mechanics principle, it is unacceptable to transfer two electrons in one step [60–63,81,90]. Moreover, the use of electrochemical impedance spectroscopy revealed the presence of adsorbed monovalent intermediate for many other metals e.g., Fe [91–94], Al [95,96], Cr [97], Zn [98,99] and Mo [100,101] and, the use of monovalent adsorbed species, to describe this relaxation phenomenon, is indeed a very common way for describing multi-electron transfer mechanisms for metal dissolution [102–105].

It should also be noticed that Mg^+ intermediate could be present as Mg^+_{ads}, $(MgOH)_{ads}$ or any other equivalent species, that can lead to the final formation of stable hydrated divalent Mg ions, depending on the Mg chemistry, electrochemistry, thermodynamics in aqueous environment, as well as the pH and potential [30]. On this aspect, a detailed description of the Mg interface with respect to corrosion products, intermediate species and their role in catalysing the anodic hydrogen evolution was recently published by Huang et al. [106].

When the initial pH of the solution is 2.9, a slightly different shape for the impedance diagram is observed (Fig. 1**b**). In the high frequency range, the time constant is attributed to the charge transfer in parallel with the interfacial capacitance [6,17]. The medium frequency time constant, which is poorly separated, may be attributed to the diffusion of species inside the Nernst diffusion layer and/or through a thin porous metastable passive layer, which is formed and dissolved under the competition between hydroxide ions formation at the Mg surface and protons provided by the bulk of the solution [3]. In the low frequency range however, an inductive loop is also observed which is again ascribed to the relaxation of adsorbed Mg^+ intermediates [6,17].

When the initial pH of the solution is more acidic, i.e., 1.8, a different shape for the impedance diagram, with three distinct time-constants, is obtained (Fig. 1**c**). In the high frequency range, the time constant is attributed to the charge transfer in parallel with the double layer capacitance only, since no hydroxide layer can be formed and the oxide layer chemically dissolved according to the reaction [3,35,107–109]:

$$MgO + 2H^+ \rightarrow Mg^{2+} + H_2O \quad (d)$$

In the medium to low frequency range, two inductive loops are observed. One can be ascribed to the relaxation of Mg^+ intermediates [6,17] and, the other to the relaxation of a second adsorbed intermediate [110]. From the impedance diagrams, it can be clearly seen that the Mg corrosion mechanism, at the early stages, is strongly dependent on the initial pH of the bulk solution and the corrosion resistance of the material is significantly diminished by one to two orders of magnitude when the initial pH of the solution is decreased from 7.7 to 1.8 (Fig. 1). The emergence of a second inductive loop is very likely to be linked to the pH change.

To confirm this assumption, additional experiments were performed (data not shown). They consist in measuring the impedance response of the Mg electrode first, in the Na_2SO_4 solution at pH = 7.7 after 30 min of immersion at E_{corr}, and then, the solution was acidified at pH = 1.8 and a second EIS measurement was performed after again 30 min of immersion at E_{corr}. In the neutral solution, a classical three-time constants impedance diagram is obtained similarly to the diagram presented in Fig. 1**a**. When the pH is decreased, a similar diagram to the one presented in Fig. 1**c** is obtained.

This result supports the hypothesis that at low pH values, almost all the oxide/hydroxide present on the surface was dissolved. Moreover, one of the inductive loops is related to the relaxation of adsorbed Mg^+ intermediates whereas the other may be ascribed to the adsorption of protons on the magnesium surface corresponding to the cathodic reaction, i.e., the Volmer reaction.

3.1.2. *Influence of immersion time*

Electrochemical impedance measurements were performed for two immersion times (30 min and 2 h) at various pH. Since in alkaline conditions the behaviour of Mg has already been deeply investigated [1,5,6,17], our main focus in this study is on experiments performed in acidic sulphate solutions.

Fig. 2**a** and Fig. 2**b** show the impedance diagrams for the Mg electrode obtained at E_{corr} for two consecutive immersion times in the Na_2SO_4 solution at pH = 1.8 and pH = 2.9, respectively. The effect of the immersion time was limited to relatively short times to avoid a significant change of the pH of the solution. As can be seen, the impedance diagrams are almost not affected by short immersion times, regardless of the initial solution pH. The slight variations observed for the time constants can be related to the high reactivity of Mg, which is affected by minute change in pH in the vicinity of the electrode surface, showing that the pH of the solution plays an important role on the mechanism and its change as a function of time [111,112]. This was also supported by measuring the pH of a 30 mL solution (initial pH = 1.8) during 20 h with the Mg rotating electrode, at E_{corr} and Ω = 1000 rpm (Fig. 3). The pH in the bulk solution increased from 1.8 to 3.8 within 20 h, corresponding to a decrease in proton concentration by a factor of 100. However, the best way to understand the Mg corrosion mechanism using a RDE would be to measure the interfacial pH, but such measurement, as far as we know, has not been reported to date and needs further development in the field of pH sensors in combination with a rotating disk-electrode. Additionally, when a still electrode is used, monitoring of the interfacial pH remains challenging since the vigorous hydrogen evolution can affect both the stability of the sensor and the reproducibility of the results [113,114]. Thus, for now, this result is only accessible using modeling and simulations [115].

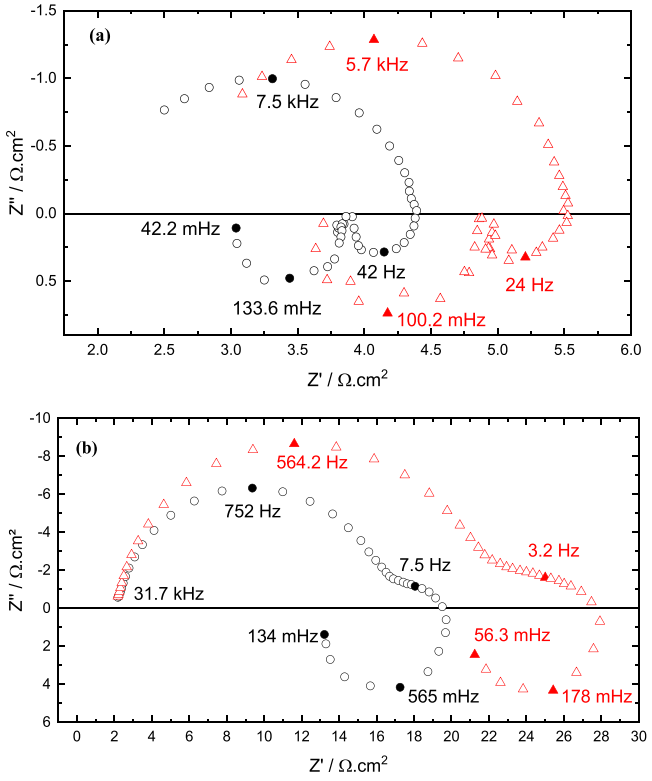

Fig. 2. Electrochemical impedance diagrams of Mg after 30 min (black circles) and 2 h (red triangles) at E_{corr} and Ω = 1000 rpm: (a) in 1 M Na_2SO_4, pH = 1.8; (b) in 1 M N Na_2SO_4, pH = 2.9.

3.1.3. *Influence of the electrode rotation rate*

Impedance diagrams obtained for two rotation rates (500 rpm and 1000 rpm) are shown in Fig. 4**a**. The shape of the impedance diagrams is unchanged with a small variation in the different time constants (amplitude of the loops). The high frequency time constants are too high to be ascribed to a diffusional process [82]. Thus, this is only related to charge transfer and the small changes observed might be directly related to the interfacial pH variation [1,5,6,17]. Interestingly, this assumption can be verified using normalized impedance diagrams [1,5,6,17] (Fig. 4**b**).

3.1.4. *Impedance diagrams in the anodic and cathodic domains*

To investigate the origin of the two inductive loops observed for the lowest pH (1.8), impedance measurements were performed at different anodic and cathodic potentials. First, Fig. 5 shows the current/potential curve, corrected from the ohmic drop, obtained for Mg in a 1 M Na_2SO_4 solution acidified at pH 1.8. The anodic and the cathodic branches were obtained from independent measurements and the different polarization potentials at which impedance measurements were performed are indicated on the curve.

The effect of the applied anodic and cathodic potentials on the Mg electrode is shown in Fig. 6**a** and Fig. 6**b**, respectively. The results clearly indicate that the mechanism, at E_{corr}, holds also for low anodic and cathodic overpotentials. However, the first inductive loop (medium frequency range) is strongly affected by both the anodic and the cathodic polarizations. In fact, the amplitude of the impedance response of the first inductive loop is decreasing with anodic potential and almost disappears for high anodic overpotentials. This shows that this time constant should be ascribed to a cathodic process, very likely to the

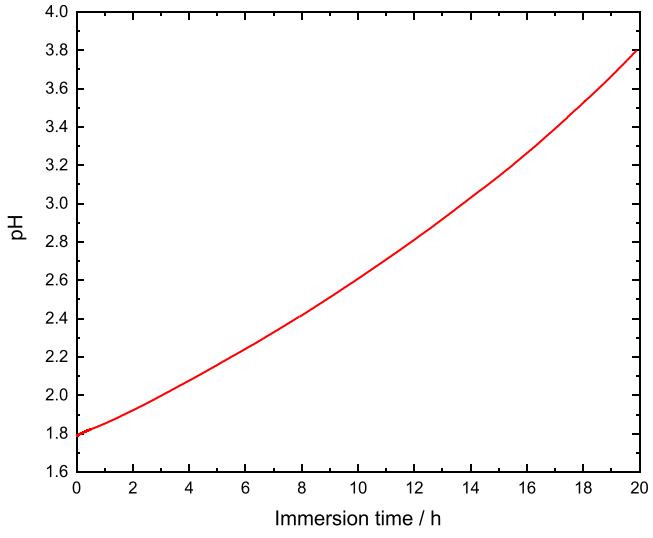

Fig. 3. Change of the pH of the Na_2SO_4 solution (volume of 30 mL) during 20 h immersion of the Mg electrode at E_{corr} and Ω = 1000 rpm.

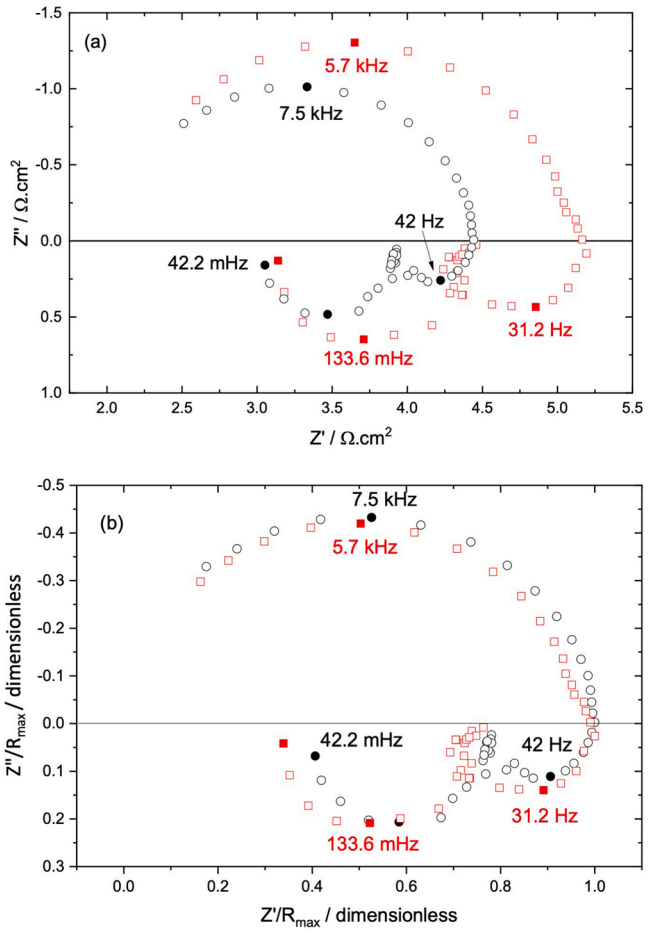

Fig. 4. Nyquist plots of the impedance response at two different rotation rates (Ω = 500 rpm (black circles) and Ω = 1000 rpm (red squares)) of Mg after 30 min at E_{corr} in 1 M Na_2SO_4 (pH = 1.8): (a) raw impedance diagrams; (b) normalized impedance diagrams (normalized by R_{max}, the maximum of the real part of each diagram).

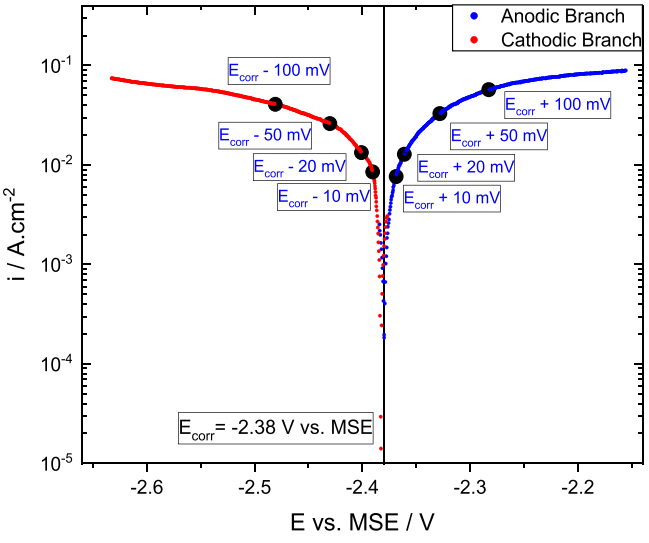

Fig. 5. Current-potential curve of Mg, corrected from the ohmic drop, measured after 30 min at E_{corr} in 1 M Na_2SO_4 acidified at pH = 1.8 (Ω = 1000 rpm, v = 0.1 mV s^{-1}).

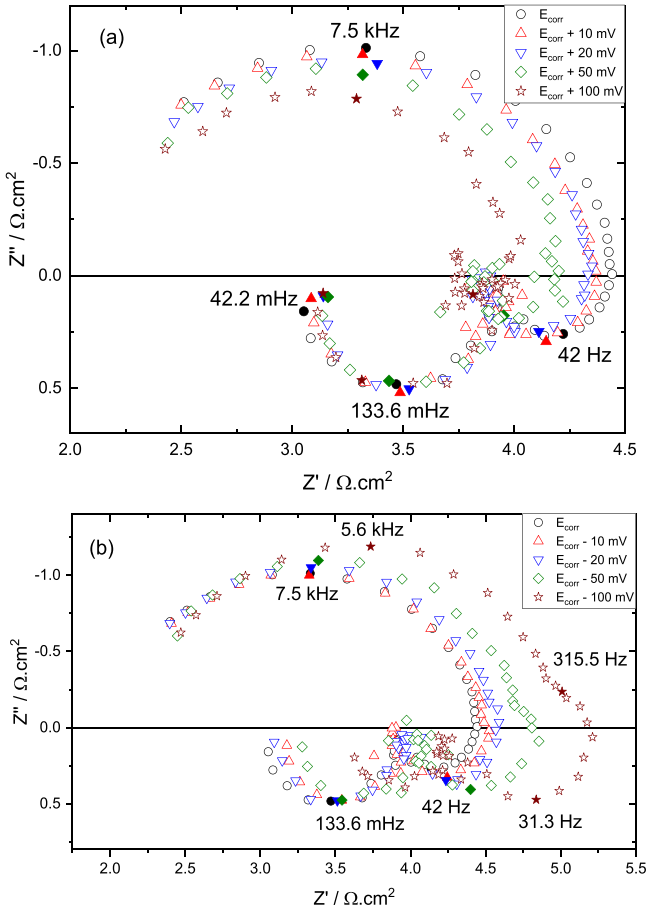

Fig. 6. Electrochemical impedance diagrams of Mg after 30 min at E_{corr} in 1 M Na_2SO_4 acidified at pH = 1.8 (Ω = 1000 rpm) at different (a) anodic and (b) cathodic overpotentials.

hydrogen evolution reaction, which occurs through the Volmer-Heyrovsky mechanism. This two steps pathway, involving the adsorption of protons, is known to be more favorable on a Mg surface than the Volmer-Tafel process [32]. By analyzing the cathodic impedance spectra, the same conclusion can be made on the contribution of cathodic and anodic reactions to the global impedance. It is important here to point out that, when the pH is increasing, the two inductive time constants overlap (Fig. 1) and at higher pH values, the cathodic contribution to the global faradic impedance becomes negligible as reported in several works [6,17] (this point will be discussed in the non-linear regression section).

Moreover, the second inductive loop (low-frequency range) is almost unchanged by the anodic polarization (Fig. 6**a**) and decreases with cathodic potential (Fig. 6**b**). This response may be related to a catalytic adsorbed intermediate (Mg_{ads}*) as postulated for iron dissolution [111, 112]. In the present work, we limit our analysis to the corrosion mechanism at the corrosion potential and for low anodic and cathodic overpotentials and the classical adsorbed intermediate (Mg_{ads}^{+}) will be used as intermediate species in our model.

3.2. Corrosion mechanism

3.2.1. Kinetics model

From the experimental results, a comprehensive model is proposed to complete the existing mechanism [1,5,6,17] and to describe the corrosion of Mg over a wide pH domain. Thus, when the pH is very low, a simplified interfacial process is described in Fig. 7**a** and, when the pH is low but, not enough to dissolve the oxide layer, one may suggest the

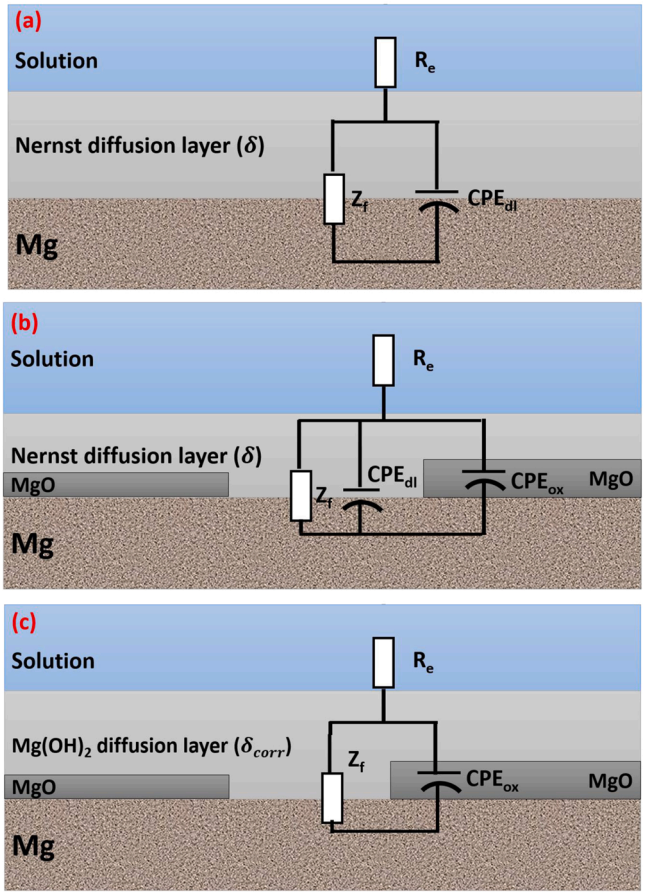

Fig. 7. Schematic representation of the Mg interface and of the equivalent circuits for: (a) very low pH, (b) low pH and (c) neutral or alkaline pH.

presence of a partially thin oxide layer (Fig. 7**b)** and the diffusion layer is ascribed to the diffusion of proton in solution (Nernst diffusion layer). In neutral to alkaline solution, the Nernst diffusion layer is replaced by the diffusion in the hydroxide layer and the interfacial capacitance is then governed by the contribution of the oxide film capacitance **(**Fig. 7**c)**. More complex equivalent circuits describing the interface, for instance taking into account the contribution of both the double layer and the oxide thin film can be used, but we represent here only the kinetically limiting elements, i.e. those from which a value can be extracted from the analysis of the diagrams.

In acidic medium and at the corrosion potential condition, the bare Mg surface is in contact with the solution and thus four anodic and cathodic partial reactions and a chemical reaction have to be considered [1,5,6,17]:

$$Mg \xrightarrow{k_1} Mg^{+}_{ads} + e^{-} \quad (1)$$

1st partial anodic *reaction*

$$Mg^{+}_{ads} \underset{k_{-2}}{\overset{k_3}{\rightleftarrows}} Mg^{2+} + e^{-} \quad (2)$$

2nd partial anodic *reaction*

$$Mg^{+}_{ads} + H^{+} \xrightarrow{k_3} Mg^{2+} + \frac{1}{2}H_2 \quad (3)$$

Chemical *reaction* (NDE)

$$H^{+} + e^{-} \xrightarrow{k_4} H_{ads} \quad (4)$$

1st partial cathodic *reaction* (Volmer *step*)

$$H_{ads} + H^{+} + e^{-} \xrightarrow{k_5} H_2 \quad (5)$$

2nd partial cathodic *reaction* (Heyrovsky *step*)

As both Nernst potentials E_{eq}(Mg) and E_{eq}(H) are apart from each other, one may neglect in the following discussion, the anodic hydrogen oxidation [81].

Although it is known that hydrogen evolution reaction can occur following two different two-step mechanisms, the Volmer-Tafel pathway and/or the Volmer-Heyrovsky pathway [81], the predominant mechanism on a Mg surface is the Volmer-Heyrovsky mechanism as shown by Yuwono et al. [32] and will be the only mechanism considered in this work. Moreover, these steps are followed either by the diffusion of H_2 from the surface to the bulk solution or by its coalescence at the surface [81], but these phenomena are disregarded since they do not contribute to the global impedance response (i.e., we assume that hydrogen bubbles do not remain on the electrode surface under the vigorous agitation of the RDE). The absorption of hydrogen into Mg is also neglected.

On the basis of the obtained results and literature, the proton discharge occurs without diffusion kinetic limitation [6]. In neutral to alkaline solutions, a corrosion layer is also formed and thus, the following reactions should be considered:

$$Mg^{+}_{ads} + H_2O \xrightarrow{k_3} Mg^{2+} + OH^{-} + \frac{1}{2}H_2 \quad (6)$$

Chemical *reaction* (NDE)

$$H_2O + e^{-} \xrightarrow{k_4} H_{ads} + OH^{-} \quad (7)$$

1st partial cathodic *reaction* (Volmer *step*)

$$H_{ads} + H_2O + e^{-} \xrightarrow{k_5} H_2 + OH^{-} \quad (8)$$

2nd partial cathodic *reaction* (Heyrovsky *step*)

At a given potential, the reduction of water occurs with a lower rate constant in comparison with the proton reduction, thus this reaction is predominant only when the proton concentration is very low [81].

The modelling and the fitting of EIS impedance diagrams were obtained by assuming that the adsorbates Mg^{+}_{ads} and H_{ads} obey a Langmuir's isotherm and that the rate constants of electrochemical reactions are exponentially potential dependent (Tafel's law). Each reaction (index i) has a normalized rate constant K_i corresponding to its rate constant k_i by [6,17]:

$$K_i = k_i e^{\pm b_i\left(E-E^0\right)} \quad (9)$$

Where b_i is the activation coefficient, and E° is the origin of potential (in this work, the corrosion potential). It is worth noting that the rate constants k_3, K_4 and K_5 include for convenience the concentration terms [116].

Let us assume that the maximum numbers of sites per surface unit that can be occupied by the adsorbates Mg^{+}_{ads} and H_{ads} are β_1 and β_2, respectively. We also assume that no competitive adsorption of other ions or dissolved species, with Mg^{+}_{ads} and H_{ads}, occurs in the studied potential range. The mass and charge balances can be expressed as functions of the fractions of the surface coverage, θ_1 and θ_2, of the adsorbed species

$$\beta_1 \frac{d\theta_1}{dt} = K_1(1-\theta_1-\theta_2) - K_2\beta_1\theta_1 + K_{-2}C_{Mg^{2+}} - k_3\beta_1\theta_1 \quad (10)$$

$$\beta_2 \frac{d\theta_2}{dt} = K_4(1-\theta_1-\theta_2) - K_5\beta_2\theta_2 \quad (11)$$

$$D\frac{C_{Mg^{2+}}}{\delta} = K_2\beta_1\theta_1 - K_{-2}C_{Mg^{2+}} + k_3\beta_1\theta_1 \quad (12)$$

Where δ is the thickness of the diffusion layer. C_{Mg2+} is the concentration of the Mg^{2+} ions at the electrode interface and, D is the diffusion

$$\frac{\Delta I_F}{FA} = (-K_1+K_4+K_2\beta_1)\Delta\theta_1 + (-K_1+K_4-K_5\beta_2)\Delta\theta_2 + ((1-\theta_1-\theta_2)(K_1b_1+K_4b_4) + \beta_2\theta_2K_5b_5 + \beta_1\theta_1K_2b_2 + C_{Mg^{2+}}K_{-2}b_{-2}]\quad \Delta V - K_{-2}\Delta C_{Mg^{2+}} \tag{22}$$

coefficient of Mg^{2+}.

Interestingly the same set of equations can be used for acidic media, neutral and alkaline media under the assumption that these reactions are not limited by mass transport of protons or water molecules and that Mg cations diffuse either inside a finite-thickness diffusion layer (the Nernst diffusion layer or inside the porous hydroxide layer depending on the pH). Thus, only the diffusion coefficient and the thickness of the diffusion layer need to be adjusted depending on the pH (Fig. 7).

The total faradic current I_F is given by

$$I_F = FA\left[K_1(1-\theta_1-\theta_2) + K_2\beta_1\theta_1 - K_{-2}C_{Mg^{2+}} - K_4(1-\theta_1-\theta_2) - K_5\beta_2\theta_2\right] \tag{13}$$

Where F is Faraday's constant, A is the electrode surface area.

At steady-state, $d\theta_1/dt = 0$ and $d\theta_2/dt = 0$, which allows to calculate the steady-state Mg^{2+} concentration $\overline{C_{Mg^{2+}}}$ and surface coverages $\overline{\theta_1}$ et $\overline{\theta_2}$ as the solution of the set of 3 linear equations with 3 unknowns:

$$K_1(1-\overline{\theta_1}-\overline{\theta_2}) - K_2\beta_1\overline{\theta_1} + K_{-2}\overline{C_{Mg^{2+}}} - k_3\beta_1\overline{\theta_1} = 0 \tag{14}$$

ΔC_{Mg2+} is the concentration variation inside a finite-thickness diffusion layer, δ, and is related to the Warburg impedance, N(ω), as [82].

$$N(\omega) = \frac{\tanh\left(\delta\sqrt{\frac{j\omega}{D}}\right)}{\sqrt{j\omega D}} \tag{23}$$

$$\frac{\Delta C_{Mg^{2+}}}{\Delta I_F} = \frac{1}{FAD}\frac{\tanh\left(\delta\sqrt{\frac{j\omega}{D}}\right)}{\sqrt{\frac{j\omega}{D}}} = \frac{1}{FA}N(\omega) \tag{24}$$

Eq. 19 thus expresses as

$$\frac{1}{Z_f} = \frac{\Delta I_F}{\Delta V} = FA((1-\theta_1-\theta_2)(K_1b_1+K_4b_4) + \beta_2\theta_2K_5b_5 + \beta_1\theta_1K_2b_2 + C_{Mg^{2+}}K_{-2}b_{-2}] + FA(-K_1+K_4+K_2\beta_1)\frac{\Delta\theta_1}{\Delta V} + FA(-K_1+K_4-K_5\beta_2)\frac{\Delta\theta_2}{\Delta V} - FAK_{-2}\frac{\Delta C_{Mg^{2+}}}{\Delta V} \tag{25}$$

$$K_4(1-\overline{\theta_1}-\overline{\theta_2}) - K_5\beta_2\overline{\theta_2} = 0 \tag{15}$$

$$D\frac{\overline{C_{Mg^{2+}}}}{\delta} = K_2\beta_1\overline{\theta_1} - K_{-2}\overline{C_{Mg^{2+}}} + k_3\beta_1\overline{\theta_1} \tag{16}$$

At steady-state, the Mg^{2+} concentration at the interface is a function of the surface coverage of the Mg^{+}_{ads}:

$$\overline{C_{Mg^{2+}}} = \frac{(K_2+k_3)\beta_1\overline{\theta_1}}{\left(\frac{D}{\delta}+K_{-2}\right)} \tag{17}$$

with

$$\overline{\theta_2} = \frac{K_4}{(K_4+K_5\beta_2)}(1-\overline{\theta_1}) \tag{18}$$

$$\overline{\theta_1} = \frac{K_1\left(\frac{D}{\delta}+K_{-2}\right)}{\frac{D}{\delta}\beta_1(K_2+k_3)\left(\frac{K_4}{K_5\beta_2}+1\right) + K_1\left(\frac{D}{\delta}+K_{-2}\right)} \tag{19}$$

The linearization of Eqs. 7, 8 and 10, for amplitude perturbations, allows to calculate the faradic admittance, $1/Z_f$

$$[\beta_1 j\omega + K_1 + \beta_1(K_2+k_3)]\Delta\theta_1 + K_1\Delta\theta_2 = [(1-\theta_1-\theta_2)K_1b_1 - \beta_1\theta_1K_2b_2 - C_{Mg^{2+}}K_{-2}b_{-2}]\Delta V + K_{-2}\Delta C_{Mg^{2+}} \tag{20}$$

$$K_4\Delta\theta_1 + (\beta_2 j\omega + K_4 + K_5\beta_2)\Delta\theta_2 = [\beta_2\theta_2K_5b_5 - (1-\theta_1-\theta_2)K_4b_4]\Delta V \tag{21}$$

Under this form, $1/Z_f$, we can clearly see the different contributions related to the charge transfer resistance (the two first terms in the right-hand side of Eq. 22), the relaxation of the two adsorbed intermediates and the contribution of the diffusion of Mg^{2+} inside the diffusion layer.

For the sake of simplicity in the global expression of the impedance, we use the following notations

$$r_1 = (1-\theta_1-\theta_2)K_1b_1 \tag{26}$$

$$r_2 = K_2b_2\beta_1\theta_1 + K_{-2}b_{-2}C_{Mg^{2+}} \tag{27}$$

$$r_4 = (1-\theta_1-\theta_2)K_4b_4 \tag{28}$$

$$r_5 = K_5b_5\beta_2\theta_2 \tag{29}$$

$$R_t = \frac{1}{FA(r_1+r_2+r_4+r_5)} \tag{30}$$

$$S_1 = \frac{(\beta_2 j\omega + K_4 + K_5\beta_2)(-K_1+K_4+K_2\beta_1) - K_4(-K_1+K_4-K_5\beta_2)}{(\beta_1 j\omega + K_1 + \beta_1(K_2+k_3))(\beta_2 j\omega + K_4 + K_5\beta_2) - K_1K_4} \tag{31}$$

$$S_2 = \frac{(\beta_1 j\omega + K_1 + \beta_1(K_2+k_3))(-K_1+K_4-K_5\beta_2) - K_1(-K_1+K_4+K_2\beta_1)}{(\beta_1 j\omega + K_1 + \beta_1(K_2+k_3))(\beta_2 j\omega + K_4 + K_5\beta_2) - K_1K_4} \tag{32}$$

The faradic impedance can thus be written as

$$Z_f = \frac{1}{FA}\frac{1 + K_{-2}N(\omega)[1 - S_1]}{(r_1 - r_2)S_1 + (r_5 - r_4)S_2 + (r_1 + r_2 + r_4 + r_5)} \quad (33)$$

$$Z_f = R_t\left\{1 + K_{-2}N(\omega) - \frac{(r_1 - r_2)S_1 + (r_5 - r_4)S_2 + K_{-2}N(\omega)[(2r_1 + r_4 + r_5)S_1 + (r_5 - r_4)S_2]}{(r_1 - r_2)S_1 + (r_5 - r_4)S_2 + (r_1 + r_2 + r_4 + r_5)}\right\} \quad (34)$$

$$Z_f = R_t\left\{\begin{array}{c} 1 + K_{-2}N(\omega) - S_1\dfrac{(r_1 - r_2) + K_{-2}(2r_1 + r_4 + r_5)N(\omega)}{(r_1 - r_2)S_1 + (r_5 - r_4)S_2 + (r_1 + r_2 + r_4 + r_5)} \\ -S_2\dfrac{(r_5 - r_4)(1 + K_{-2}N(\omega))}{(r_1 - r_2)S_1 + (r_5 - r_4)S_2 + (r_1 + r_2 + r_4 + r_5)} \end{array}\right\} \quad (35)$$

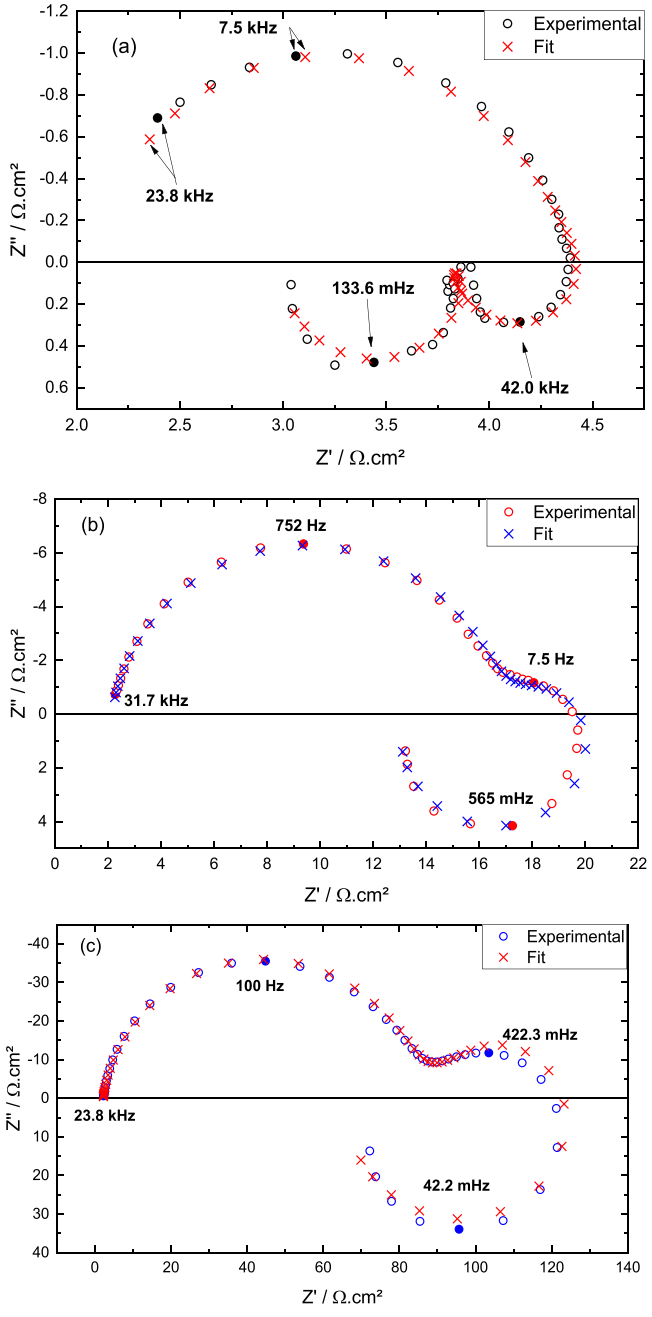

Fig. 8. Impedance diagrams of the Mg electrode after 30 min at E_{corr} in 1 M Na_2SO_4 (Ω = 1000 rpm) (blue circles) and the result of the fitting procedure with the model (Eqs. (30) and (33)) (red crosses) at (a) pH = 1.8, (b) pH = 2.9, and (c) pH = 7.7.

The global impedance, *Z*, can then be obtained by taking into account the electrolyte resistance and the interfacial capacitance (the double layer or the thin oxide film contribution), which is considered as a CPE element to account for the non-ideal behaviour of the experimental results [82].

$$Z = R_e + \frac{Z_f \times Z_{CPE}}{Z_f + Z_{CPE}} \quad (36)$$

in which, the CPE impedance is defined as

$$Z_{CPE} = \frac{1}{Q(j\omega)^{\alpha}} \quad (37)$$

where *Q* has units of Ω^{-1} cm^{-2} s^{α} and α is the CPE exponent [82].

Interestingly, if the impedance response is dominated by the anodic branch (contribution of the cathodic reaction is neglected), a similar expression to that reported in [6,17] is obtained.

3.2.2. Non-linear regression

The fitting was performed using a home-made software based on a non-linear regression. The diffusion coefficient at pH = 1.8 and pH = 2.9 was fixed at $D = 7.06\ 10^{-6}$ cm^2 s^{-1} [117] whereas at pH = 7.7, it was obtained from the fitting procedure. Because experiments in low pH solutions can only be performed for short immersion times, we assume that the diffusion layer is the Nernst diffusion layer, which was calculated [82] for pH = 1.8 and pH = 2.9 using the rotation rate of the electrode and fixed at $\delta = 15.7$ μm for the fitting procedure, whereas for

Table 1
Parameters obtained from the regression of the EIS experimental data.

	pH = 1.8	pH = 2.9	pH = 7.7
k_1 / mol cm^{-2} s^{-1}	8.07 10^{-6}	1.09 10^{-7}	1.00 10^{-9}
b_1 / V^{-1}	30.0	20.0	15.2
k_2 / s^{-1}	9.00 10^{-1}	8.05 10^{-1}	2.80 10^{-3}
b_2 / V^{-1}	7.6	6.8	4.9
k_{-2} / cm s^{-1}	1.38 10^{-2}	3.27 10^{-3}	5.61 10^{-4}
b_{-2} / V^{-1}	2.0	2.0	7.5
k_3 / s^{-1}	1.00 10^{-1}	9.93 10^{-2}	1.00 10^{-2}
k_4 / mol cm^{-2} s^{-1}	2.61 10^{-4}	3.01 10^{-6}	3.31 10^{-7}
b_4 / V^{-1}	15.0	8.7	8.1
k_5 / s^{-1}	1.26 10^{-1}	2.62 10^{-2}	4.95 10^{-3}
b_5 / V^{-1}	34.9	22.0	21.8
D / cm^2 s^{-1}	7.06 10^{-6}	7.06 10^{-6}	9.07 10^{-7}
δ / μm	15.7	15.7	20.0
Q_{ox} / Ω^{-1} cm^{-2} s^{α}	–	1.02 10^{-5}	2.98 10^{-5}
α_{ox}	–	0.938	0.921
Q_{dl} / Ω^{-1} cm^{-2} s^{α}	1.20 10^{-5}	2.12 10^{-5}	4.24 10^{-7}
α_{dl}	0.907	0.893	0.922
R_{ox} / Ω cm^2	–	95.30	1.00 10^{10}
R_e / Ω cm^2	2.05	2.15	2.23
β_1 / mol cm^{-2}	5.7 10^{-7}	7.5 10^{-7}	1.0 10^{-6}
β_2 / mol cm^{-2}	6.1 10^{-7}	7.6 10^{-7}	8.9 10^{-7}
θ_1	3 10^{-3}	2.8 10^{-3}	2 10^{-3}
θ_2	0.997	0.993	0.985
$C_{Mg^{2+}}$ / mol L^{-1}	1 10^{-7}	8 10^{-8}	3 10^{-8}

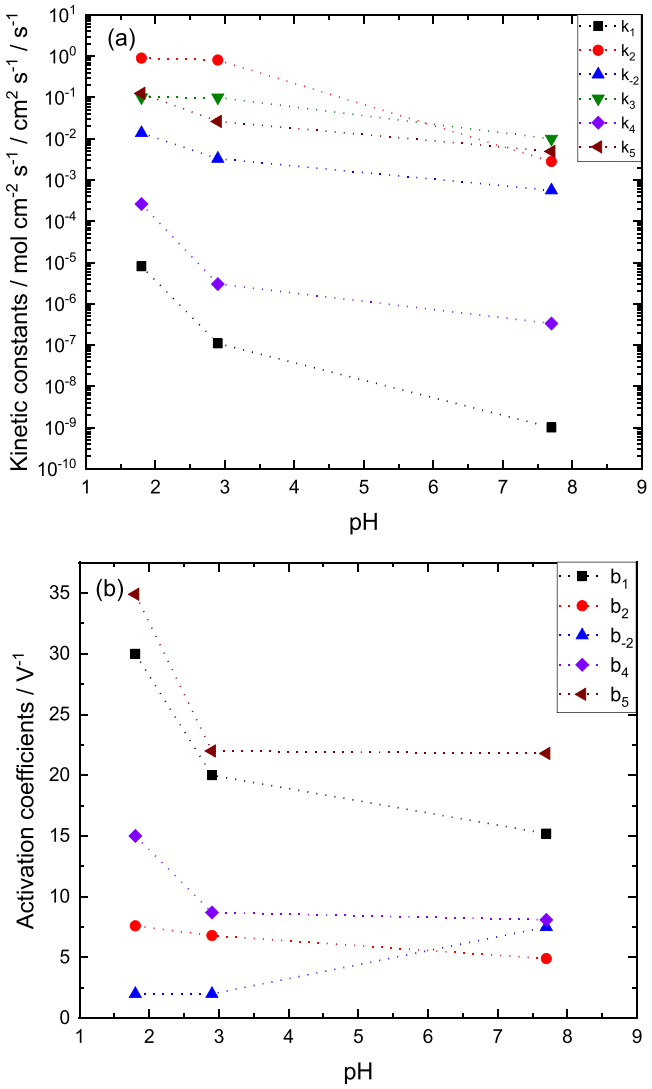

Fig. 9. Variations of the different kinetic parameters related to the corrosion of the Mg electrode after 30 min at E_{corr} in 1 M Na_2SO_4 (Ω = 1000 rpm) as function of the pH: (a) kinetic constants and (b) activation coefficients.

longer immersion times and neutral or alkaline pH, the thickness of the corrosion product layer at pH = 7.7 was obtained from the fitting. All the other parameters were also obtained from the fitting procedure.

Fig. 8 compares the experimental Nyquist plots and the spectra obtained from the non-linear regression using the proposed model for different pH values. The experimental data are in good agreement with the regression curves.

The different parameters obtained from the regression of the EIS experimental data are reported in Table 1 for the different pH.

From the fitting procedure, the thickness of the $Mg(OH)_2$ corrosion product layer formed in 1 M Na_2SO_4 at an initial pH 7.7 after 30 min, was estimated at a few micrometers, in agreement with the fast formation of a thick layer in the early stages, when Mg is in contact with a neutral to slightly alkaline media. The diffusion coefficient in the above-mentioned case, was estimated at 9.07 10^{-7} cm^2 s^{-1}, which indirectly underlines the high porosity of the corrosion product layer in its early stages of the corrosion process. The surface coverage, θ_2, by the H_{ads} adsorbates is very high and decreases from 99.7% to 98.5% by changing the solution pH from 1.8 to 7.7. This shows that H is strongly adsorbed on the surface even for high pH values and for anodic polarizations. For the surface coverage by the Mg^+_{ads} adsorbates, θ_1 deceased from 3 10^{-3} to 2 10^{-3} when the pH is increased from 1.8 to 7.7. The interfacial concentration of Mg^{2+} ions is very low and also decreased from 1 10^{-7} to 3 10^{-8} mol L^{-1}. The variation of the kinetic constants and the activation coefficients is given in Fig. 9.

Globally, all the time constants are decreasing when the pH increases, which is in agreement with the increase of the corrosion resistance in alkaline solution. Interestingly, the parameter k_{-2}, which was initially introduced in the model to take into account the effect of the diffusion, decreased by almost one order of magnitude each time the pH is increased, from 1.8 to 2.9 and then to 7.7. This may explain the appearance of a diffusional time constant, starting from a pH of 2.9, which becomes well-formed for higher pH values, at neutral to slightly alkaline pH. All the Tafel coefficients are decreasing except b_{-2} which increases from 2 to 7.5.

Regarding the constant phase element parameters, it is only for higher pH values that the double layer capacitance contribution can be neglected, whereas for lower pH, the contribution of the oxide film on the bare electrode is disregarded. The difficulty when doing the fit is the deconvolution between these two capacitive contributions, and a comprehensive method should be used for this aim as was recently demonstrated for the case of aluminium [118]. Thus, the obtained values can be regarded as effective values related to both contributions and at this stage the equivalent capacities cannot be estimated easily. As a result, in low pH domain, the double layer capacitance can be linked to the active surface area.

4. Conclusions

In the present work, electrochemical impedance diagrams obtained for a Mg rotating disk electrode in a sodium sulphate solution at three different pH values (1.8, 2.9 and 7.7) were analysed and discussed by considering not only the anodic dissolution, as it has been done usually in the literature, but also the cathodic reaction. On the basis of the experimental data and from the literature review, a comprehensive model was proposed to complete the existing corrosion mechanism of Mg [1,5,6,17] and thus, to fully describe all the time constants observed on the impedance diagrams at the corrosion potential as a function of pH. Two anodic and two cathodic partial reactions and a chemical reaction were considered. The simulated impedance diagrams were in good agreement with the experimental data. The two inductive loops observed for low pH values were attributed to the presence of adsorbed intermediates, most likely H_{ads} and Mg^+_{ads} in the middle and low frequency ranges, respectively. Interestingly, taking into account few assumptions, the proposed mechanism can be used for all pH values. The corrosion mechanism of Mg is governed by the presence (at high pH value) or not (at low pH value) of a $MgO/Mg(OH)_2$ layer. The key points of the model are the following:

1. The diffusion occurs within a diffusion layer, the Nernst diffusion layer when no hydroxide layer is present on the surface, or inside the porous hydroxide layer when the pH of precipitation is reached.
2. The contribution of the double layer is much pronounced in the case of a bare Mg surface and becomes negligible when an oxide/hydroxide layer is present on the surface.
3. The contribution of the cathodic partial reactions is to be considered only in highly acidic medium and becomes negligible at higher pH values. In other words, the corrosion mechanism is dominated by the anodic branch only when the pH is neutral to alkaline.
4. Another explanation is that either the reduction of the protons or water molecules is catalysed by the presence of the oxide/hydroxide layer [119]. On this aspect, it is well-known that some metal oxides such as MgO and Al_2O_3 are maximal valence oxides, whose cations are in their highest valence state, and thus their surfaces are quite inert in chemisorption, involving an electron transfer from the oxide to the adsorbed molecule since their cations are not able to supply electrons by oxidation [81].

CRediT authorship contribution statement

Abdelmoheiman Zakaria Benbouzid: Investigation, Methodology, Writing. **Maurilio Pereira Gomes:** Investigation, **Isolda Costa:** Writing – review & editing., **Jesualdo Luiz Rossi:** Writing – review & editing. **Oumaïma Gharbi**: Writing – review & editing. **Nadine Pébère:** Conceptualization, Methodology, Investigation, Writing – review & editing. **Mai T.T. Tran:** Conceptualization, Methodology, Investigation, Writing – review & editing., **Bernard Tribollet:** Conceptualization, Methodology, Investigation, Writing – review & editing. **Mireille Turmine, Vincent Vivier:** Conceptualization, Methodology, Investigation, Writing – review & editing.

Declaration of Competing Interest

The authors declare that they have no known competing financial interests or personal relationships that could have appeared to influence the work reported in this paper.

Data Availability

Data will be made available on request.

Acknowledgments

Abdelmoheiman Zakaria Benbouzid acknowledges Ecole Militaire Polytechnique d'Alger, Algeria for his PhD grant. Maurilio Pereira Gomes acknowledges FAPESP (2013/13235-6) and CAPES-Cofecub (806-14) for the financial support to this research (grant 88881.154406/2017-01).

AZB thanks Abdelilah Asserghine for providing beneficial discussion and useful comments.

References

[1] N. Pebere, C. Riera, F. Dabosi, Investigation of magnesium corrosion in aerated sodium sulfate solution by electrochemical impedance spectroscopy, Electrochim. Acta 35 (1990) 555–561, https://doi.org/10.1016/0013-4686(90)87043-2.
[2] R. Udhayan, D.P. Bhatt, On the corrosion behaviour of magnesium and its alloys using electrochemical techniques, J. Power Sources 63 (1996) 103–107, https://doi.org/10.1016/S0378-7753(96)02456-1.
[3] G. Song, A. Atrens, D. Stjohn, J. Nairn, Y. Li, The electrochemical corrosion of pure magnesium in 1 N NaCl, Corros. Sci. 39 (1997) 855–875, https://doi.org/10.1016/S0010-938X(96)00172-2.
[4] G. Song, A. Atrens, D. John St., X. Wu, J. Nairn, The anodic dissolution of magnesium in chloride and sulphate solutions, Corros. Sci. 39 (1997) 1981–2004, https://doi.org/10.1016/S0010-938X(97)00090-5.
[5] G. Baril, N. Pébère, Corrosion of pure magnesium in aerated and deaerated sodium sulphate solutions, Corros. Sci. 43 (2001) 471–484, https://doi.org/10.1016/S0010-938X(00)00095-0.
[6] G. Baril, G. Galicia, C. Deslouis, N. Pébère, B. Tribollet, V. Vivier, An impedance investigation of the mechanism of pure magnesium corrosion in sodium sulfate solutions, J. Electrochem. Soc. 154 (2007) C108, https://doi.org/10.1149/1.2401056.
[7] S. Bender, J. Goellner, A. Atrens, Corrosion of AZ91 in 1N NaCl and the mechanism of magnesium corrosion, Adv. Eng. Mater. 10 (2008) 583–587, https://doi.org/10.1002/adem.200800005.
[8] Z. Shi, A. Atrens, An innovative specimen configuration for the study of Mg corrosion, Corros. Sci. 53 (2011) 226–246, https://doi.org/10.1016/j.corsci.2010.09.016.
[9] N.T. Kirkland, G. Williams, N. Birbilis, Observations of the galvanostatic dissolution of pure magnesium, Corros. Sci. 65 (2012) 5–9, https://doi.org/10.1016/j.corsci.2012.08.029.
[10] Z. Shi, F. Cao, G.L. Song, A. Atrens, Low apparent valence of Mg during corrosion, Corros. Sci. 88 (2014) 434–443, https://doi.org/10.1016/j.corsci.2014.07.060.
[11] L. Rossrucker, K.J.J. Mayrhofer, G.S. Frankel, N. Birbilis, Investigating the real time dissolution of mg using online analysis by ICP-MS, J. Electrochem. Soc. 161 (2014) C115–C119, https://doi.org/10.1149/2.064403jes.
[12] A.D. King, N. Birbilis, J.R. Scully, Accurate electrochemical measurement of magnesium corrosion rates; a combined impedance, mass-loss and hydrogen collection study, Electrochim. Acta 121 (2014) 394–406, https://doi.org/10.1016/j.electacta.2013.12.124.
[13] V. Shkirskiy, A.D. King, O. Gharbi, P. Volovitch, J.R. Scully, K. Ogle, N. Birbilis, Revisiting the electrochemical impedance spectroscopy of magnesium with online inductively coupled plasma atomic emission spectroscopy, ChemPhysChem 16 (2015) 536–539, https://doi.org/10.1002/cphc.201402666.
[14] S. Lebouil, O. Gharbi, P. Volovitch, K. Ogle, Mg dissolution in phosphate and chloride electrolytes: Insight into the mechanism of the negative difference effect, Corrosion 71 (2015) 234–241, https://doi.org/10.5006/1459.
[15] K.D. Ralston, S. Thomas, G. Williams, N. Birbilis, An electrochemical quartz crystal microbalance study of magnesium dissolution, Appl. Surf. Sci. 360 (2016) 342–348, https://doi.org/10.1016/j.apsusc.2015.11.040.
[16] S. Fajardo, O. Gharbi, N. Birbilis, G.S. Frankel, Investigating the effect of ferrous ions on the anomalous hydrogen evolution on magnesium in acidic ferrous chloride solution, J. Electrochem. Soc. 165 (2018) C916–C925, https://doi.org/10.1149/2.0951813jes.
[17] M.P. Gomes, I. Costa, N. Pébère, J.L. Rossi, B. Tribollet, V. Vivier, On the corrosion mechanism of Mg investigated by electrochemical impedance spectroscopy, Electrochim. Acta 306 (2019) 61–70, https://doi.org/10.1016/j.electacta.2019.03.080.
[18] S. Bender, J. Goellner, A. Heyn, S. Schmigalla, A new theory for the negative difference effect in magnesium corrosion, Mater. Corros. 63 (2012) 707–712, https://doi.org/10.1002/maco.201106225.
[19] G.L. Song, A. Atrens, Corrosion mechanisms of magnesium alloys, Adv. Eng. Mater. 1 (1999) 11–33, https://doi.org/10.1002/(SICI)1527-2648(199909)1:1<11::AID-ADEM11>3.0.CO;2-N.
[20] G. Song, A. Atrens, Understanding magnesium corrosion—a framework for improved alloy performance, Adv. Eng. Mater. 5 (2003) 837–858, https://doi.org/10.1002/adem.200310405.
[21] G. Song, Recent progress in corrosion and protection of magnesium alloys, Adv. Eng. Mater. 7 (2005) 563–586, https://doi.org/10.1002/adem.200500013.
[22] G. Song, A. Atrens, Recent insights into the mechanism of magnesium corrosion and research suggestions, Adv. Eng. Mater. 9 (2007) 177–183, https://doi.org/10.1002/adem.200600221.
[23] A. Atrens, W. Dietzel, The negative difference effect and unipositive Mg, Adv. Eng. Mater. 9 (2007) 292–297, https://doi.org/10.1002/adem.200600275.
[24] A. Atrens, G.L. Song, F. Cao, Z. Shi, P.K. Bowen, Advances in Mg corrosion and research suggestions, J. Magnes. Alloy. 1 (2013) 177–200, https://doi.org/10.1016/j.jma.2013.09.003.
[25] S. Thomas, N.V. Medhekar, G.S. Frankel, N. Birbilis, Corrosion mechanism and hydrogen evolution on Mg, Curr. Opin. Solid State Mater. Sci. 19 (2015) 85–94, https://doi.org/10.1016/j.cossms.2014.09.005.
[26] A. Atrens, G.-L. Song, M. Liu, Z. Shi, F. Cao, M.S. Dargusch, Review of recent developments in the field of magnesium corrosion, Adv. Eng. Mater. 17 (2015) 400–453, https://doi.org/10.1002/adem.201400434.
[27] F. Cao, G.L. Song, A. Atrens, Corrosion and passivation of magnesium alloys, Corros. Sci. 111 (2016) 835–845, https://doi.org/10.1016/j.corsci.2016.05.041.
[28] M. Esmaily, J.E. Svensson, S. Fajardo, N. Birbilis, G.S. Frankel, S. Virtanen, R. Arrabal, S. Thomas, L.G. Johansson, Fundamentals and advances in magnesium alloy corrosion, Prog. Mater. Sci. 89 (2017) 92–193, https://doi.org/10.1016/j.pmatsci.2017.04.011.
[29] A. Atrens, G.L. Song, Z. Shi, A. Soltan, S. Johnston, M.S. Dargusch, Understanding the corrosion of mg and mg alloys. in: Encyclopedia of Interfacial Chemistry: Surface Science and Electrochemistry, Elsevier,, 2018, pp. 515–534, https://doi.org/10.1016/B978-0-12-409547-2.13426-2.
[30] J. Huang, G.L. Song, A. Atrens, M. Dargusch, What activates the Mg surface—a comparison of Mg dissolution mechanisms, J. Mater. Sci. Technol. 57 (2020) 204–220, https://doi.org/10.1016/j.jmst.2020.03.060.
[31] A.D. Atrens, I. Gentle, A. Atrens, Possible dissolution pathways participating in the Mg corrosion reaction, Corros. Sci. 92 (2015) 173–181, https://doi.org/10.1016/j.corsci.2014.12.004.
[32] J.A. Yuwono, N. Birbilis, K.S. Williams, N.V. Medhekar, Electrochemical stability of magnesium surfaces in an aqueous environment, J. Phys. Chem. C. 120 (2016) 26922–26933, https://doi.org/10.1021/acs.jpcc.6b09232.
[33] M. Taheri, R.C. Phillips, J.R. Kish, G.A. Botton, Analysis of the surface film formed on Mg by exposure to water using a FIB cross-section and STEM-EDS, in: Corrosion Science, 59, 2012, pp. 222–228, https://doi.org/10.1016/j.corsci.2012.03.001.
[34] M. Taheri, M. Danaie, J.R. Kish, TEM examination of the film formed on corroding mg prior to breakdown, J. Electrochem. Soc. 161 (2014) C89–C94, https://doi.org/10.1149/2.017403jes.
[35] L. Wang, D. Snihirova, M. Deng, C. Wang, B. Vaghefinazari, G. Wiese, M. Langridge, D. Höche, S.V. Lamaka, M.L. Zheludkevich, Insight into physical interpretation of high frequency time constant in electrochemical impedance spectra of Mg, Corros. Sci. 187 (2021), 109501, https://doi.org/10.1016/j.corsci.2021.109501.
[36] J.A. Yuwono, C.D. Taylor, G.S. Frankel, N. Birbilis, S. Fajardo, Understanding the enhanced rates of hydrogen evolution on dissolving magnesium, Electrochem. Commun. 104 (2019), 106482, https://doi.org/10.1016/j.elecom.2019.106482.
[37] J.A. Yuwono, N. Birbilis, C.D. Taylor, K.S. Williams, A.J. Samin, N.V. Medhekar, Aqueous electrochemistry of the magnesium surface: thermodynamic and kinetic profiles, Corros. Sci. 147 (2019) 53–68, https://doi.org/10.1016/j.corsci.2018.10.014.
[38] K.S. Williams, J.P. Labukas, V. Rodriguez-Santiago, J.W. Andzelm, First principles modeling of water dissociation on Mg(0001) and development of a Mg surface Pourbaix diagram, Corrosion 71 (2015) 209–223, https://doi.org/10.5006/1322.
[39] K.S. Williams, V. Rodriguez-Santiago, J.W. Andzelm, Modeling reaction pathways for hydrogen evolution and water dissociation on magnesium, Electrochim. Acta 210 (2016) 261–270, https://doi.org/10.1016/j.electacta.2016.04.128.

[40] C.D. Taylor, A first-principles surface reaction kinetic model for hydrogen evolution under cathodic and anodic conditions on magnesium, J. Electrochem. Soc. 163 (2016) C602–C608, https://doi.org/10.1149/2.1171609jes.

[41] C.D. Taylor, Atomistic modeling of corrosion events at the interface between a metal and its environment, Int. J. Corros. (2012) (2012), https://doi.org/10.1155/2012/204640.

[42] C.D. Taylor, M. Neurock, Theoretical insights into the structure and reactivity of the aqueous/metal interface, Curr. Opin. Solid State Mater. Sci. 9 (2005) 49–65, https://doi.org/10.1016/j.cossms.2006.03.007.

[43] M.E. Straumanis, B.K. Bhatia, Disintegration of magnesium while dissolving anodically in neutral and acidic solutions, J. Electrochem. Soc. 110 (1963) 357, https://doi.org/10.1149/1.2425763.

[44] J.L. Robinson, P.F. King, Electrochemical behavior of the magnesium anode, J. Electrochem. Soc. 108 (1961) 36, https://doi.org/10.1149/1.2428007.

[45] B. Tribollet, G. Galicia, N. Pebere, V. Vivier, Corrosion study of an AZ91 magnesium alloy by EIS and LEIS, ECS Trans. 1 (2019) 157–168, https://doi.org/10.1149/1.2215499.

[46] L. Rossrucker, A. Samaniego, J.-P. Grote, A.M. Mingers, C.A. Laska, N. Birbilis, G. S. Frankel, K.J.J. Mayrhofer, The pH dependence of magnesium dissolution and hydrogen evolution during anodic polarization, J. Electrochem. Soc. 162 (2015) C333–C339, https://doi.org/10.1149/2.0621507jes.

[47] W.J. James, M.E. Straumanis, B.K. Bhatia, J.W. Johnson, The difference effect on magnesium dissolving in acids, J. Electrochem. Soc. 110 (1963) 1117, https://doi.org/10.1149/1.2425601.

[48] Y. Li, Z. Shi, X. Chen, A. Atrens, Anodic hydrogen evolution on Mg, J. Magnes. Alloy. 9 (2021) 2049–2062, https://doi.org/10.1016/j.jma.2021.09.002.

[49] M.C. Zhao, M. Liu, G.L. Song, A. Atrens, Influence of pH and chloride ion concentration on the corrosion of Mg alloy ZE41, Corros. Sci. 50 (2008) 3168–3178, https://doi.org/10.1016/j.corsci.2008.08.023.

[50] S. Johnston, Z. Shi, A. Atrens, The influence of pH on the corrosion rate of high-purity Mg, AZ91 and ZE41 in bicarbonate buffered Hanks' solution, Corros. Sci. 101 (2015) 182–192, https://doi.org/10.1016/j.corsci.2015.09.018.

[51] O. Gharbi, N. Birbilis, Clarifying the dissolution mechanisms and electrochemistry of Mg 2 Si as a Function of Solution pH, J. Electrochem. Soc. 165 (2018) C497–C501, https://doi.org/10.1149/2.1061809jes.

[52] A. Maltseva, V. Shkirskiy, G. Lefèvre, P. Volovitch, Effect of pH on Mg(OH) 2 film evolution on corroding Mg by in situ kinetic Raman mapping (KRM), Corros. Sci. 153 (2019) 272–282, https://doi.org/10.1016/j.corsci.2019.03.024.

[53] J.W. Turrentine, Reversed electrolysis, J. Phys. Chem. 12 (1908) 448–467, https://doi.org/10.1021/j150096a006.

[54] R.L. Petty, A.W. Davidson, J. Kleinberg, The anodic oxidation of magnesium metal: evidence for the existence of unipositive magnesium, J. Am. Chem. Soc. 76 (1954) 363–366, https://doi.org/10.1021/ja01631a013.

[55] T.R. Thomaz, C.R. Weber, T. Pelegrini, L.F.P. Dick, G. Knörnschild, The negative difference effect of magnesium and of the AZ91 alloy in chloride and stannate-containing solutions, Corros. Sci. 52 (2010) 2235–2243, https://doi.org/10.1016/j.corsci.2010.03.010.

[56] C. Do Lee, C.S. Kang, K.S. Shin, Effects of chunk breakage and surface protective film on negative difference effect of magnesium alloys, Met. Mater. Int. 7 (2001) 385–391, https://doi.org/10.1007/bf03186084.

[57] R. Tunold, H. Holtan, M.B.H. Berge, A. Lasson, R. Steen-Hansen, The corrosion of magnesium in aqueous solution containing chloride ions, Corros. Sci. 17 (1977) 353–365, https://doi.org/10.1016/0010-938X(77)90059-2.

[58] A. Samaniego, B.L. Hurley, G.S. Frankel, On the evidence for univalent Mg, J. Electroanal. Chem. 737 (2015) 123–128, https://doi.org/10.1016/j.jelechem.2014.04.013.

[59] S. Al Bacha, A. Desmedt, M. Zakhour, M. Nakhl, J.L. Bobet, Mechanism of hydrogen formation during the corrosion of Mg17Al12, Electrochem. Commun. 119 (2020), 106813, https://doi.org/10.1016/J.ELECOM.2020.106813.

[60] H. Ma, X.Q. Chen, R. Li, S. Wang, J. Dong, W. Ke, First-principles modeling of anisotropic anodic dissolution of metals and alloys in corrosive environments, Acta Mater. 130 (2017) 137–146, https://doi.org/10.1016/j.actamat.2017.03.027.

[61] H. Ma, M. Liu, W. Chen, C. Wang, X.Q. Chen, J. Dong, W. Ke, First-principles study on the effects of twin boundaries on anodic dissolution of Mg, Phys. Rev. Mater. 3 (2019), 053806, https://doi.org/10.1103/PhysRevMaterials.3.053806.

[62] T. Würger, C. Feiler, G.B. Vonbun-Feldbauer, M.L. Zheludkevich, R.H. Meißner, A first-principles analysis of the charge transfer in magnesium corrosion, Sci. Rep. 10 (2020) 1–11, https://doi.org/10.1038/s41598-020-71694-4.

[63] H. Ma, L. Wu, C. Liu, M. Liu, C. Wang, D. Li, X.Q. Chen, J. Dong, W. Ke, First-principles modeling of the hydrogen evolution reaction and its application in electrochemical corrosion of Mg, Acta Mater. 183 (2020) 377–389, https://doi.org/10.1016/j.actamat.2019.11.025.

[64] W. Jeffrey Binns, F. Zargarzadah, V. Dehnavi, J. Chen, J.J. Noël, D.W. Shoesmith, Physical and electrochemical evidence for the role of a Mg hydride species in Mg alloy corrosion, Corrosion 75 (2019) 58–68, https://doi.org/10.5006/2918.

[65] T. Jiang, L.X. Sun, W.X. Li, First-principles study of hydrogen absorption on Mg (0001) and formation of magnesium hydride, Phys. Rev. B - Condens. Matter Mater. Phys. 81 (2010), 035416, https://doi.org/10.1103/PhysRevB.81.035416.

[66] A. Seyeux, M. Liu, P. Schmutz, G. Song, A. Atrens, P. Marcus, ToF-SIMS depth profile of the surface film on pure magnesium formed by immersion in pure water and the identification of magnesium hydride, Corros. Sci. 51 (2009) 1883–1886, https://doi.org/10.1016/j.corsci.2009.06.002.

[67] T. Hiraki, S. Hiroi, T. Akashi, N. Okinaka, T. Akiyama, Chemical equilibrium analysis for hydrolysis of magnesium hydride to generate hydrogen, Int. J. Hydrog. Energy 37 (2012) 12114–12119, https://doi.org/10.1016/j.ijhydene.2012.06.012.

[68] J. Chen, J. Dong, J. Wang, E. Han, W. Ke, Effect of magnesium hydride on the corrosion behavior of an AZ91 magnesium alloy in sodium chloride solution, Corros. Sci. 50 (2008) 3610–3614, https://doi.org/10.1016/j.corsci.2008.09.013.

[69] W.D. Mueller, H. Hornberger, The influence of MgH2 on the assessment of electrochemical data to predict the degradation rate of Mg and Mg alloys, Int. J. Mol. Sci. 15 (2014) 11456–11472, https://doi.org/10.3390/ijms150711456.

[70] G.G. Perrault, Potentiostatic study of the magnesium electrode in aqueous solution, J. Electroanal. Chem. 27 (1970) 47–58, https://doi.org/10.1016/S0022-0728(70)80201-7.

[71] G.S. Frankel, A. Samaniego, N. Birbilis, Evolution of hydrogen at dissolving magnesium surfaces, Corros. Sci. 70 (2013) 104–111, https://doi.org/10.1016/j.corsci.2013.01.017.

[72] S. Fajardo, G.S. Frankel, Effect of impurities on the enhanced catalytic activity for hydrogen evolution in high purity magnesium, Electrochim. Acta 165 (2015) 255–267, https://doi.org/10.1016/j.electacta.2015.03.021.

[73] D. Lysne, S. Thomas, M.F. Hurley, N. Birbilis, On the Fe enrichment during anodic polarization of mg and its impact on hydrogen evolution, J. Electrochem. Soc. 162 (2015) C396–C402, https://doi.org/10.1149/2.0251508jes.

[74] M. Taheri, J.R. Kish, N. Birbilis, M. Danaie, E.A. McNally, J.R. McDermid, Towards a physical description for the origin of enhanced catalytic activity of corroding magnesium surfaces, Electrochim. Acta 116 (2014) 396–403, https://doi.org/10.1016/j.electacta.2013.11.086.

[75] B. Roald, W. Beck, The dissolution of magnesium in hydrochloric acid, J. Electrochem. Soc. 98 (1951) 277, https://doi.org/10.1149/1.2778207.

[76] H.H. Uhlig, R. Krutenat, Formation of dissolved atomic hydrogen by electrochemical polarization, J. Electrochem. Soc. 111 (1964) 1303, https://doi.org/10.1149/1.2425990.

[77] E.J. Casey, R.E. Bergeron, On the mechanism of the dissolution of magnesium in acidic salt solutions: i. Physical control by surface films, Can. J. Chem. 31 (1953) 849–867, https://doi.org/10.1139/v53-115.

[78] P.F. King, The role of the anion in the anodic dissolution of magnesium, J. Electrochem. Soc. 113 (1966) 536, https://doi.org/10.1149/1.2424019.

[79] H.A. Robinson, Magnesium as a galvanic anode, Trans. Electrochem. Soc. 90 (1946) 485, https://doi.org/10.1149/1.3071762.

[80] E.J. Casey, R.E. Bergeron, G.D. Nagy, On the mechanism of dissolution of magnesium in aqueous magnesium chloride solutions: part II, Can. J. Chem. 40 (1962) 463–479, https://doi.org/10.1139/v62-074.

[81] P. Marcus, ed., Corrosion Mechanisms in Theory and Practice, CRC Press, 2011. https://doi.org/10.1201/b11020.

[82] M.E. Orazem, B. Tribollet, Electrochemical Impedance. Spectroscopy, John Wiley & Sons, Inc,, Hoboken, NJ, USA, 2008, https://doi.org/10.1002/9780470381588.

[83] J. Chen, Y. Song, D. Shan, E.H. Han, Study of the corrosion mechanism of the in situ grown Mg-Al-CO 32- hydrotalcite film on AZ31 alloy, Corros. Sci. 65 (2012) 268–277, https://doi.org/10.1016/j.corsci.2012.08.026.

[84] F. Cao, Z. Shi, G.L. Song, M. Liu, M.S. Dargusch, A. Atrens, Influence of casting porosity on the corrosion behaviour of Mg0.1Si, Corros. Sci. 94 (2015) 255–269, https://doi.org/10.1016/j.corsci.2015.02.002.

[85] H. Xu, X. Zhang, K. Zhang, Y. Shi, J. Ren, Effect of extrusion on corrosion behavior and corrosion mechanism of Mg-Y alloy, J. Rare Earths 34 (2016) 315–327, https://doi.org/10.1016/S1002-0721(16)60031-5.

[86] J. Li, B. Zhang, Q. Wei, N. Wang, B. Hou, Electrochemical behavior of Mg-Al-Zn-In alloy as anode materials in 3.5 wt% NaCl solution, Electrochim. Acta 238 (2017) 156–167, https://doi.org/10.1016/j.electacta.2017.03.119.

[87] H. Pan, L. Wang, Y. Lin, F. Ge, K. Zhao, X. Wang, Z. Cui, Mechanistic study of ammonium-induced corrosion of AZ31 magnesium alloy in sulfate solution, J. Mater. Sci. Technol. 54 (2020) 1–13, https://doi.org/10.1016/j.jmst.2020.02.074.

[88] C. Gabrielli, M. Keddam, H. Takenouti, Kramers-Kronig transformation in relation to the interface regulating device, in: J.R. Scully, D.C. Silverman, M.W. Kendig (Eds.), Electrochemical Impedance: Analysis and Interpretation, ASTM International, West Conshohocken, PA, 1993, pp. 140–153, https://doi.org/10.1520/STP18067S.

[89] M.T.M. Koper, Thermodynamic theory of multi-electron transfer reactions: Implications for electrocatalysis, J. Electroanal. Chem. 660 (2011) 254–260, https://doi.org/10.1016/j.jelechem.2010.10.004.

[90] J. Bockris, A. Reddy, Modern electrochemistry, Plenum Press,, New York, 1977, 6th printing.

[91] E.J. Kelly, The active iron electrode, J. Electrochem. Soc. 112 (1965) 124, https://doi.org/10.1149/1.2423480.

[92] E.J. Kelly, The active iron electrode, J. Electrochem. Soc. 115 (1968) 1111, https://doi.org/10.1149/1.2410920.

[93] I. Epelboin, C. Gabrielli, M. Keddam, H. Takenouti, A model of the anodic behaviour of iron in sulphuric acid medium, Electrochim. Acta 20 (1975) 913–916, https://doi.org/10.1016/0013-4686(75)87017-4.

[94] T. Chagas-Almeida, O.E. Barcia, R.M. Moreira, M.C.E. Bandeira, O.R. Mattos, Discussion and challenges concerning the elaboration of a dissolution reaction mechanism, Electrochim. Acta 303 (2019) 211–218, https://doi.org/10.1016/j.electacta.2019.02.036.

[95] D.D. Macdonald, S. Real, S.I. Smedley, M. Urquidi-Macdonald, Evaluation of Alloy Anodes For Aluminum-air Batteries: Iv. Electrochemical Impedance Analysis Of Pure Aluminum In At 25°c, J. Electrochem. Soc. 135 (1988) 2410–2414, 10.1149/1.2095348d.d.

[96] L. Bai, B.E. Conway, Complex behavior of Al dissolution in non-aqueous medium as revealed by impedance spectroscopy, J. Electrochem. Soc. 137 (1990) 3737–3747, https://doi.org/10.1149/1.2086295.
[97] J.A.L. Dobbelaar, J.H.W. de Wit, Impedance measurements and analysis of the corrosion of chromium, J. Electrochem. Soc. 137 (1990) 2038–2046, https://doi.org/10.1149/1.2086861.
[98] C. Cachet, F. Ganne, G. Maurin, J. Petitjean, V. Vivier, R. Wiart, EIS investigation of zinc dissolution in aerated sulfate medium. Part I: Bulk zinc, Electrochim. Acta 47 (2001) 509–518, https://doi.org/10.1016/S0013-4686(01)00740-X.
[99] C. Cachet, F. Ganne, S. Joiret, G. Maurin, J. Petitjean, V. Vivier, R. Wiart, EIS investigation of zinc dissolution in aerated sulphate medium. Part II: Zinc coatings, Electrochim. Acta 47 (2002) 3409–3422, https://doi.org/10.1016/S0013-4686(02)00277-3.
[100] M. Bojinov, I. Betova, R. Raicheff, Transpassivity of molybdenum in H2SO4 solution, J. Electroanal. Chem. 381 (1995) 123–131, https://doi.org/10.1016/0022-0728(94)03675-S.
[101] M. Bojinov, I. Betova, R. Raicheff, A model for the transpassivity of molybdenum in acidic sulphate solutions based on ac impedance measurements, Electrochim. Acta 41 (1996) 1173–1179, https://doi.org/10.1016/0013-4686(95)00468-8.
[102] R.D. Armstrong, M. Henderson, Impedance plane display of a reaction with an adsorbed intermediate, J. Electroanal. Chem. 39 (1972) 81–90, https://doi.org/10.1016/S0022-0728(72)80477-7.
[103] I. Epelboin, M. Keddam, J.C. Lestrade, Faradaic impedances and intermediates in electrochemical reactions, Faraday Discuss. Chem. Soc. 56 (1973) 264–275, https://doi.org/10.1039/DC9735600264.
[104] J. Maddala, K. Sambath, V. Kumar, S. Ramanathan, Identification of reaction mechanism for anodic dissolution of metals using Electrochemical Impedance Spectroscopy, J. Electroanal. Chem. 638 (2010) 183–188, https://doi.org/10.1016/j.jelechem.2009.11.021.
[105] D. Klotz, Negative capacitance or inductive loop? – a general assessment of a common low frequency impedance feature, Electrochem. Commun. 98 (2019) 58–62, https://doi.org/10.1016/j.elecom.2018.11.017.
[106] J. Huang, G.L. Song, Y. Zhu, D. Zheng, Z. Wang, The anodically polarized Mg surface products and accelerated hydrogen evolution, J. Magnes. Alloy. (2021), https://doi.org/10.1016/J.JMA.2021.05.008.
[107] A. Fedoročková, P. Raschman, Effects of pH and acid anions on the dissolution kinetics of MgO, Chem. Eng. J. 143 (2008) 265–272, https://doi.org/10.1016/j.cej.2008.04.029.
[108] L.F. Amaral, I.R. Oliveira, R. Salomão, E. Frollini, V.C. Pandolfelli, Temperature and common-ion effect on magnesium oxide (MgO) hydration, Ceram. Int. 36 (2010) 1047–1054, https://doi.org/10.1016/j.ceramint.2009.12.009.
[109] G.G. Perrault, The potential-pH diagram of the magnesium-water system, J. Electroanal. Chem. 51 (1974) 107–119, https://doi.org/10.1016/S0022-0728(74)80298-6.
[110] A. Lasia, Impedance spectroscopy applied to the study of electrocatalytic processes. in: Encyclopedia of Interfacial Chemistry: Surface Science and Electrochemistry, Elsevier,, 2018, pp. 241–263, https://doi.org/10.1016/B978-0-12-409547-2.13361-X.
[111] M. Keddam, O.R. Mottos, H. Takenouti, Reaction model for iron dissolution studied by electrode impedance: i. Experimental results and reaction model, J. Electrochem. Soc. 128 (1981) 257–266, https://doi.org/10.1149/1.2127401.
[112] M. Keddam, O.R. Mattos, H. Takenouti, Reaction model for iron dissolution studied by electrode impedance: ii. Determination of the reaction model, J. Electrochem. Soc. 128 (1981) 266–274, https://doi.org/10.1149/1.2127402.
[113] J. Izquierdo, B.M. Fernández-Pérez, D. Filotás, Z. Őri, A. Kiss, R.T. Martín-Gómez, L. Nagy, G. Nagy, R.M. Souto, Imaging of concentration distributions and hydrogen evolution on corroding magnesium exposed to aqueous environments using scanning electrochemical microscopy, Electroanalysis 28 (2016) 2354–2366, https://doi.org/10.1002/elan.201600265.
[114] D. Filotás, B.M. Fernández-Pérez, L. Nagy, G. Nagy, R.M. Souto, A novel scanning electrochemical microscopy strategy for the investigation of anomalous hydrogen evolution from AZ63 magnesium alloy, Sens. Actuators, B: Chem. 308 (2020), 127691, https://doi.org/10.1016/j.snb.2020.127691.
[115] E.B. Carneiro-Neto, M.C. Lopes, E.C. Pereira, Simulation of interfacial pH changes during hydrogen evolution reaction, J. Electroanal. Chem. 765 (2016) 92–99, https://doi.org/10.1016/j.jelechem.2015.09.029.
[116] J. Diard, B. Le Gorrec, C. Montella, Discussion of first-order inductive impedance for the Volmer-Heyrovsky mechanism, J. De. Chim. Phys. 92 (1995) 656–667, https://doi.org/10.1051/jcp/1995920656.
[117] Y. Marcus, Ions Solut. Their Solvation (2015) 1–293, https://doi.org/10.1002/9781118892336.
[118] O. Gharbi, M.T.T. Tran, M.E. Orazem, B. Tribollet, M. Turmine, V. Vivier, Impedance Response of a thin film on an electrode: deciphering the influence of the double layer capacitance, ChemPhysChem 22 (2021) 1371–1378, https://doi.org/10.1002/cphc.202100177.
[119] S.H. Salleh, S. Thomas, J.A. Yuwono, K. Venkatesan, N. Birbilis, Enhanced hydrogen evolution on Mg (OH)2 covered Mg surfaces, Electrochim. Acta 161 (2015) 144–152, https://doi.org/10.1016/j.electacta.2015.02.079.